

Cite this: *J. Mater. Chem. B*, 2025, 13, 7428

Chromogenic ecdysis of Au@Ag nanorods assembled in a hydrogel for selective detection of ammonia vapors in food†

Mahima Chandel,^a Prem Singh,[‡] Kamaljit Kaur,[‡] Lalitya Chadalawada,^a T. S. Abhijith,^a Keshav Bhardwaj,[§] Amit Jaiswal[§]*^b and Vijayakumar Shanmugam[§]*^a

Chromogenic sensors are highly appreciated, but the color change must be significant to clearly indicate the change. We proposed a hydrogel sensor containing Au-bead@Ag nanorods for the detection of ammonia to ascertain the shelflife of meat. Polymers with different water-holding capacity were tested. Agarose gel had the required amount of water to capture ammonia to show a significant visible color change as a function of different ammonia concentrations. Microscopy and X-ray photoemission spectroscopy (XPS) showed the captured ammonia tuned the pH to dissolve Ag in Au-bead@Ag nanorods into ions/clusters/alloys for the color change. The color changed from orange to blue-green in the gel after 3 h of exposure to an ammonia-spiked meat sample.

Received 20th March 2025,
Accepted 8th May 2025

DOI: 10.1039/d5tb00636h

rsc.li/materials-b

1. Introduction

Each year, approximately one-third of food produced goes to waste, which contributes to one-third of greenhouse gases released. Conversely, a WHO report has stated that contaminated food is responsible for approximately 600 million cases of illness and around 420 000 deaths globally.¹ Hence, there is a need to reduce the waste to ensure food security and environmental sustainability.² Therefore, real-time visual monitoring of food quality can guarantee food safety as well as minimize food wastage by pricing in a proportion-to-perishability index.

Protein-rich food such as meat and tofu is prone to microbial contamination, which causes the release of ammonia in small quantities at an early stage.³ Several analytical methods, such as radiofrequency identification tags,⁴ electronic noses,⁵ and chemoresistive gas sensors,⁶ are available to detect ammonia, but their complex processing, relatively high cost of manufacturing and complicated instrumentation limit their practical uses. Therefore, development of a colorimetric sensor, which gives real-time on-site monitoring of food spoilage, is of

great interest.^{7–9} In the past few years, colorimetric sensors based on chromogenic reagents have been used for the detection of ammonia and other biogenic amines.^{10–13} However, the use of these chromogenic substrates cause low color resolution, leaching as well as more time needed for color changes.¹¹ Recently, in biosensors, the adoption of nanoparticles to develop stable colorimetric methods is increasing.^{14–16}

Hence, to develop a stable chromogenic platform, plasmon-rich silver and gold nanoparticles have been used for the detection of analytes by changing the matrix. In the absence of an analyte, the particles disperse freely in the matrix whereas, in the presence of the analyte, the matrix reacts to aggregate the nanoparticles. The functional groups on the particles/matrix have found to be critical for: (i) the metal ion detection using sensor array of cysteine, L-glutathione, and melamine capping;¹⁷ (ii) detection of organophosphate pesticides and ion concentrations in NaCl with optimum pH;¹⁸ (iii) physiological phosphate detection of thiol cations.¹⁹ Thus, a combination of organic groups + ions and their reaction with an analyte to change the pH or hydrogen bond or ionic strength can result in the development of chromogenic sensing. In this well-established aggregation-induced chromogenic change, the missing model is dissolution of the shell-induced plasmon-rich core aggregation into the sensor. Conversely, a monolayer of organic content on plasmonic particles and its catalytic reactivity and high sensitivity has been appreciated for chromogenic sensors without aggregation.²⁰

Hence, it would be interesting to ascertain the role of a thin shell in sensing. However, the challenge of demonstrating this

^a Institute of Nano Science and Technology, Knowledge City, Sahibzada Ajit Singh Nagar, Punjab 140306, India. E-mail: vijayakumarshanmugam@gmail.com

^b School of Biosciences and Bioengineering, Indian Institute of Technology Mandi, Kamand, Mandi 175005, Himachal Pradesh, India. E-mail: j.amit@iitmandi.ac.in

^c University Institute of Engineering and Technology, Panjab University, 160014 Chandigarh, India

† Electronic supplementary information (ESI) available. See DOI: <https://doi.org/10.1039/d5tb00636h>

‡ These authors contributed equally to this work.

model practically is to select a shell that can be fragile to volatile ammonia. Hence, herein Au-bead@Ag nanorods were selected as the Au core with Ag as a thin shell. Additionally, the redox-unstable Ag coating enabled rapid dissolution in volatile ammonia for the visual change. Hydrogels have recently gained significant attention due to their three-dimensional porous structures, excellent hydrophilicity, and ease of use.²¹ Growing evidence supports their practical applications in wound dressings,²² bone regeneration,²³ as well as for the delivery of nutrients, flavoring agents, bioactive compounds, or semisolid ingredients in low-fat food formulations.²⁴ Therefore, considering the numerous advantages of hydrogels, in the present study, Au-bead@Ag nanorods were incorporated in an agarose hydrogel for ammonia detection. This system exhibited a consistent color change upon exposure to ammonia vapors, caused by the dissolution of the Ag coating. An excellent chromogenic sensor was developed, thanks to the gel being able to efficiently adsorb and react with the analyte to embed particles in the gel.^{25–27} Au-bead@Ag nanorods showed great signal transduction through the change in aspect ratio after ammonia exposure in proportion to the change in the localized surface plasmon resonance (LSPR) peak. Overall, the proposed sensor offers various advantages over a reported non-destructive, instrument-free, high-resolution colorimetric method with simple fabrication and ease of use.²⁸ Additionally, a low cost, reproducibility, lack of interference, and no pretreatment make this sensor robust for practical applications. Furthermore, use of the sensor in food samples ensures its practical applicability.

2. Experimental section

2.1 Materials

Chloroauric acid (HAuCl_4), benzyldimethylhexadecylammonium chloride (BDAC), citric acid, sodium borohydride (NaBH_4), and L-ascorbic acid were purchased from Merck Sigma. Agarose, sodium alginate, trimethylamine, and morpholine were obtained from SRL, polyvinyl alcohol (PVA) and calcium chloride were from Himedia, hexadecyltrimethylammonium chloride (CTAC), and carboxymethyl cellulose–sodium (CMC–Na) was sourced from TCI, ammonia, benzylamine, hydrazine, and pyrrolidine were procured from Merck Sigma, and tapioca starch was purchased from Jioo Organics, all of which were used without further modifications. A meat sample was bought from a local market in Mohali.

2.2 Synthesis of Au-bead@Ag nanorods

Au-bead@Ag nanorods were synthesized in accordance with a procedure reported previously.²⁹ Briefly, Au seed was prepared by reducing HAuCl_4 with a strong reducing agent, NaBH_4 , in the presence of a cationic surfactant (CTAC) and citric acid. The resulting seed solution was thermally treated to obtain twinned particles. These twinned particles were used to prepare gold beads employing BDAC as a surfactant, HAuCl_4 as a gold precursor, and ascorbic acid as a reducing agent. Then, silver deposition on gold beads was pursued using CTAC as the

capping agent, AgNO_3 as the silver source, and ascorbic acid as the reducing agent under constant magnetic stirring at 60 °C. This approach yielded uniform and monodispersed Ag nanorods, with the centrally positioned core Au bead (Au-bead@Ag nanorods).

2.3 Fabrication of a portable hydrogel

Initially, five hydrogels were synthesized: 30% PVA, 5% CMC–Na, 5% sodium alginate with calcium chloride (crosslinking agent), 25% starch, and 1% agarose; these concentrations were required for gel formation. Water was used as a solvent along with heating for the formation of gels. Au-bead@Ag nanorods were incorporated in the hydrogel when the temperature became bearable. Only agarose gel with Au-bead@Ag nanorods showed a color change after exposure to ammonia solution, so further experiments were limited to this gel only. Briefly, 1% agarose was made in boiling water and an Au-bead@Ag nanorods solution (0.5 mL, 1 mL) was added into agarose solution when it cooled down to ~40 °C. This sensory hydrogel was then transferred into the snap cap of a microcentrifuge tube (2 mL) to make it user-friendly in handling.

2.4 Characterizations

Au-bead@Ag nanorods, before being incorporated into the hydrogel, were characterized using UV-visible-NIR diffuse reflectance spectroscopy (DRS) by a spectrophotometer (Cary 5000; Agilent Technologies) to measure the LSPR peak as well as through X-ray photoemission spectroscopy (XPS). XPS was done using a surface analyser (K-alpha; Thermo Scientific) with a micro-focused (400 μm , 72 W, 12 000 V) monochromatic Al-K α source ($h\nu = 1486.6$ eV), a hemispherical analyser, and a 128-channel plate detector. After formation of the hydrogel sensor and its exposure to ammonia, the hydrogel was characterized by cryo-transmission electron microscopy (CryoTEM) using an electron microscope (TEM-2100 Plus), field emission scanning electron microscopy (FESEM) using a JSM-7610F system, atomic force microscopy (AFM) in tapping mode using an atomic force microscope (NanoScope 9.1, MultiMode 8; Bruker) and XPS. FT-IR spectroscopy was done using a spectrometer (Vortex 70; Bruker) in attenuated total reflection (ATR) mode. The mechanical strength of hydrogels exposed/not exposed to ammonia was calculated from a storage modulus vs. frequency sweep curve obtained using a rheometer (MCR302; Anton Parr) equipped with a 25-mm parallel-plate geometry. The refractive index was checked using a refractometer (Labart) and digital photographs were obtained using the camera of a smartphone (Galaxy A51; Samsung).

2.5 Visual monitoring of ammonia vapors by a portable hydrogel sensor

To detect ammonia using this hydrogel sensor, it was exposed to different concentrations (13.4 M, 10.72 M, 8.04 M, 5.36 M, 2.68 M, 0.53 M, 0.26 M) of ammonia derived from different dilutions of ammonia solution. Briefly, 1 mL of different concentrations of ammonia solution was meticulously added to the bottom of the tube, avoiding direct contact with the

sensory hydrogel placed in the snap cap of a microcentrifuge tube. This method ensured that the sensor remained uncontaminated while allowing for the detection of ammonia from the solution. Following the closure of the snap cap, the microcentrifuge tube was positioned upright at room temperature (25 °C). This setup facilitated the generation of an atmosphere rich in ammonia vapor, enabling the permeation of ammonia vapor into the sensory hydrogel. The color evolution of the hydrogel sensor was then monitored with time, and images were captured using the camera of a smartphone. Obtained digital photos were then analyzed using imageJ software to obtain the red-green-blue (RGB) values. The prepared hydrogel sensor was also checked with different types of interfering molecule (benzylamine, trimethylamine, pyrrolidine, hydrazine, and morpholine) at a concentration of 9 M because they have been postulated to be released from spoiled meat, shrimps and crab.³⁰ We wished to determine the optimal concentration of Au-bead@Ag nanorods for clear color contrast. Hence, the color change of an agarose hydrogel exposed to ammonia after incorporating different volumes of Au-bead@Ag nanorods was also documented along with rheological measurements. Two ratios of agarose (C) and Au-bead@Ag nanorods (B), named as “B (1:0.5) mL” and “B (1:1) mL”, were employed. Hydrogels were expressed as “C” (control-agarose), “CT” (control-agarose exposed to ammonia), “B” (control-agarose with Au-bead@Ag nanorods) and “BT” (control-agarose with Au-bead@Ag nanorods exposed to ammonia). Furthermore, detection of ammonia using the designed hydrogel sensor was also studied under varying temperature and humid conditions to assess its practicality in different environmental settings.

2.6 Analysis of real samples

To check the practicality of the sensor, the performance was assessed using chicken samples spiked with different concentrations of ammonia. Briefly, 2 g of a sample of minced chicken was weighed and transferred to a 15-mL centrifuge tubes. The chicken samples were then spiked with different concentrations (0.53 M, 2.68 M, 8.04 M and 13.4 M) of ammonia and vortex-mixed for 30 s. The samples were then centrifuged at 10 000 rpm for 3 min, and the supernatant was placed in a 2-mL microcentrifuge tube.³¹ The latter was analyzed employing the same procedure described in Section 2.5. Besides, the hydrogel sensor was also kept separately in a snap cap of a microcentrifuge tube in a tray containing 250 g of a chicken sample to prevent direct contact with chicken. The color change was observed periodically up to 24 h at room temperature (25 °C) and 40% relative humidity (RH).

2.7 Statistical analysis

All statistical data analysis were performed using OriginPro 2024 and ImageJ.

3. Results and discussion

This study focuses on the development of a visual sensor for ammonia detection, aimed at enabling real-time monitoring of food quality. The sensor was designed such that the dissolution

of the Ag shell and subsequent aggregation of the Au core and Au–Ag hybrid structures induced a distinct and visible color change, allowing the easy detection of ammonia.

3.1 Characterization of Au-bead@Ag nanorods

Au bead nanoparticles were synthesized using a seed-mediated growth, as reported previously.²⁹ The Au-bead@Ag nanorods were synthesised by growing Ag shells on an Au bead template. We used AgNO₃ as a precursor, CTAC as a surface capping agent, and ascorbic acid as a reducing agent. The absorbance of the as-synthesized Au-bead@Ag nanorods was characterized using UV-vis-NIR spectroscopy (Fig. 1A). UV-Vis-NIR spectroscopy revealed the presence of LSPR peak maxima for Au-bead@Ag nanorods at four zones: 1007 nm for the longitudinal mode SPR for the Ag shell; 396 nm for the transverse mode SPR for the Ag shell; around 492 nm for the transverse Au core bead; 566 nm longitudinal SPR for the Au core bead. Au and Ag have similar lattice constants (JCPDS: 4-0783 and 4-0784), so the d spacing and 2θ values were the same. It was hard to distinguish the presence of Au and Ag planes in the XRD pattern of Au-bead@Ag nanorods. However, the prominent diffraction peaks at 38.5° (111), 45.3° (200), 64.5° (220), and 77.4° (311) might have originated from the corresponding planes in a face-centred cubic (fcc) crystal structure of Au and Ag^{32–35} (Fig. S1, ESI[†]). The TEM image of Au-bead@Ag nanorods is given in Fig. 1B with energy dispersive X-ray spectrometry (EDX) confirming the presence of Au and Ag (Fig. S2, ESI[†]).

3.2 Visual monitoring of ammonia by a portable sensory hydrogel

The synthesized Au-bead@Ag nanorods were incorporated into an agarose-based hydrogel to develop a portable sensor for ammonia detection. The suitability of agarose as a matrix for this application was established after evaluating five types of hydrogels with varying water content (*vide infra*). Following this assessment, agarose gel embedded with Au-bead@Ag nanorods was selected as the optimal material for ammonia sensing. This hydrogel was enclosed in a microcentrifuge tube and exposed to different concentrations of ammonia vapors at room temperature (25 °C) and 40% RH (Fig. 1C, inset). We chose 1% agarose for hydrogel formation because a further increase in concentration led to reduced transparency (Fig. S3A, ESI[†]) and porosity. This concentration was optimal for ensuring optical clarity, uniform dispersion, oxidation of nanoparticles (*vide infra*) and easy diffusion of ammonia. Increasing the concentration further led to a longer time for the color change after ammonia exposure, as illustrated in Fig. S3B (ESI[†]). To ascertain the optimal ratio of agarose and Au-bead@Ag nanorods particles (8.37 × 10¹¹ particles mL⁻¹ concentration) for maximum color contrast, a series of volume ratios were used from 1:0.5 to 1:1 (mL). The color contrast improved as the ratio approached 1:1, so this ratio, referred to as “B (1:1) mL”, was chosen for subsequent experiments (Fig. S4, ESI[†]). Furthermore, at higher concentrations, Au-bead@Ag nanorods tended to aggregate, whereas at concentrations below 10¹¹ particles mL⁻¹, the storage modulus was reduced, as illustrated in Fig. S5 (ESI[†]).

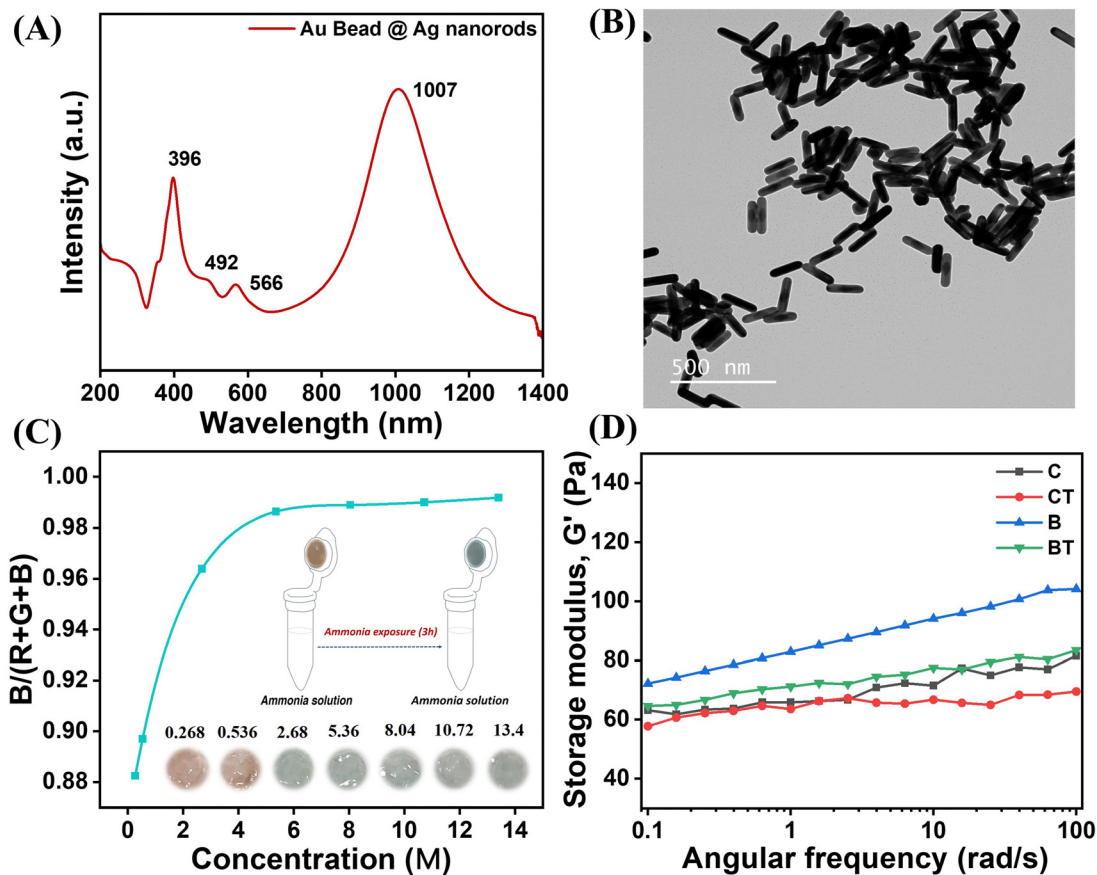


Fig. 1 (A) UV-Vis-NIR spectra of Au-bead@Ag nanorods. (B) TEM image of Au-bead@Ag nanorods. (C) Quantitative detection of ammonia vapors at room temperature (25 °C) and 40% RH by analyzing $B/(R + G + B)$ ratios from digital images. The inset is a schematic showing the color change of the hydrogel sensor from orange to blue-green after ammonia exposure. (D) Mechanical strength of the hydrogel sensor before and after exposure to ammonia. C: control hydrogel (*i.e.*, agarose); CT: control agarose hydrogel exposed to ammonia vapors; B: control-agarose hydrogel with Au-bead@Ag nanorods and BT control-agarose hydrogel with Au-bead@Ag nanorods exposed to ammonia vapors.

Notably, control hydrogels lacking Au-bead@Ag nanorods did not exhibit a color change even after prolonged exposure to ammonia vapors, indicating their inherent stability against ammonia vapors (Fig. S4, ESI[†]). The color change of the sensory hydrogel from orange to blue-green was found to be proportional to both ammonia vapor concentration and exposure time. The color of sensory hydrogel B (1 : 1) mL changed from orange to blue-green after around 180 min under high concentration of ammonia vapors (~13.4 M) (Fig. 1C, inset). Furthermore, the concentration of ammonia vapors was also determined quantitatively from the digital photographs of the hydrogel sensor by analyzing the ratio of blue intensity to the sum of red, green and blue intensity ($R + G + B$ intensity), as shown in Fig. 1C. Furthermore, the color transition of the hydrogel sensor upon exposure to ammonia across a temperature range of -20 °C to 40 °C and relative humidity from 40% to 80% demonstrated that the sensor responded more quickly – shifting from orange to blue-green – under higher temperature and humidity (Fig. S6 and S7, ESI[†]). The underlying reason for this behavior is explained below.

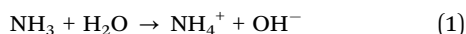
3.3 Mechanism behind chromogenic change

Different gels prepared using 30% PVA, 5% CMC-Na, 5% sodium alginate + calcium, 25% starch and 1% agarose incorporated with

Au-bead@Ag nanorods were tested for ammonia detection at room temperature (25 °C) and 40% RH. Only agarose gel with Au-bead@Ag nanorods showed a color change from orange to blue-green after exposure to ammonia solution (Fig. S8, ESI[†]). This may have been due to the ability of agarose gel to hold Au-bead@Ag nanorods with optimum rigidity at a high ratio of water for the maximum ammonia reaction at the first stage to furnish the next step of gel and plasmon particles collapse. A similar specificity of the hydrogel with different polysaccharides has been noted before for efficient capture, loading and release.³⁶

3.3.1 Gel collapse. The collapse in the mechanical strength of the gel was determined by a rheometer equipped with a 25-mm parallel-plate geometry. Both in the control gel (C) as well as gel containing Au-bead@Ag nanorods (B), a loss of storage modulus was observed after ammonia treatment (Fig. 1D). The incorporation of Au-bead@Ag nanorods into the agarose gel led to improvement in the structural integrity of the gel (B), likely due to reinforcement by the nanorods with the crosslinking network.^{37,38} This integrity decreased after ammonia treatment, which may have been because of the interference with crosslinkers (BT). In the control gel (C), the integrity was comparatively less, possibly due to the absence of the reinforcement by particles, which also showed a slight decline in integrity after ammonia treatment.

3.3.2 Particle collapse. The water within the hydrogel reacted with ammonia giving rise to ammonium ions, as shown in eqn (1):



This reaction increased the pH of the hydrogel from 10.3 to 12.7 which, in turn, led to the collapse of the primary assembly or shape or size of Au-bead@Ag nanorods, ultimately causing a visible chromogenic change (Table S1, ESI[†]). To validate this phenomenon, FESEM of freeze-dried hydrogel samples after ammonia exposure was conducted. The results revealed that ammonia exposure weakened the structural integrity of the particle assembly significantly, which was evident in comparison with the initial homogeneous distribution (Fig. 2A and B). Furthermore, CryoTEM of gel samples showed a reduction in the thickness or mass of the Ag shell, with post-exposure samples displaying quasi-spherical structures instead of nanorods (Fig. 2C and D). These observations were further corroborated by AFM, whereby distinct nanorods embedded within the gel matrix were visible before ammonia exposure, while aggregated structures were observed after ammonia exposure (Fig. S9, ESI[†]).

The change in particle morphology accompanied with aggregation gave rise to random plasmon coupling. The intensity of longitudinal mode SPR at 1007 nm and transverse mode SPR at 400 nm for the Ag shell decreased sharply with blue shift after incorporation of Au-bead@Ag nanorods within the gel. This phenomenon depicted the reaction of the Ag shell in an oxidizing gel to cause structural collapse. Furthermore, ammonia exposure led to red shift in LSPR peaks of the Au core, which was evident from the appearance of peaks at 515 nm and 618 nm, in the UV-visible-NIR spectra. The structure deformation and aggregation of the Au core led to plasmon coupling and a caused red shift (Fig. 3A).³⁹

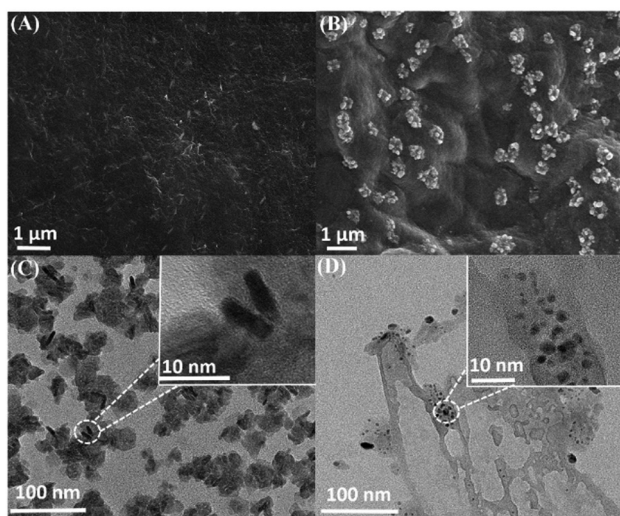


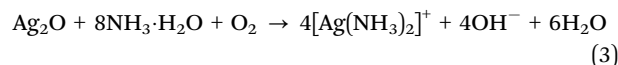
Fig. 2 FESEM and CryoTEM images (A) and (C) of B (control-agarose hydrogel with Au-bead@Ag nanorods) and (B) and (D) BT (control-agarose hydrogel with Au-bead@Ag nanorods) exposed to ammonia vapors, respectively.

Furthermore, the crowding of the particles was expected to cause fluctuation in the refractive index. As expected, the refractometer readings of the hydrogel containing Au-bead@Ag nanorods increased from ~ 2 to ~ 4 after ammonia exposure, causing shifts to a longer wavelength (Fig. S10, ESI[†]). Finally, the change in the composition was examined using XPS. The wide survey XPS spectrum of as-synthesized Au-bead@Ag nanorods verified the presence of Ag. This made up the shell around the Au core, while carbon, nitrogen, oxygen and chlorine originated from the CTAC capping agent (Fig. 3B). Narrow peaks at 367.1 and 373 eV corresponding to Ag 3d_{5/2} and Ag 3d_{3/2}, respectively, confirmed the presence of Ag in its metallic state as it was before incorporation into the gel (Fig. 3C). In this as-synthesized sample, the signal for Au was absent, which could have been because of the limitation of XPS to probe only the surface. The doublet for Au 4f electrons appeared at 82.9 and 86.6 eV after etching only (Fig. 3D). The peaks of Au and Ag shifted slightly from the actual peaks of their metallic forms due to alloy formation of AuAg at the interface, which caused charge redistribution in Au and Ag atoms.⁴⁰

After incorporating Au-bead@Ag nanorods into the hydrogel, the Ag shell underwent oxidation, converting from its metallic state to the oxidized form (Ag⁺). This transformation was facilitated by the presence of water within the gel matrix and the oxidizing environment surrounding it (eqn (2)). Under high humidity, the increased water content accelerated the oxidation of Ag, leading to a faster color change in the sensor (Fig. S7, ESI[†]).



Upon ammonia exposure, Ag becomes oxidized due to more basic conditions, leading to corrosion and subsequent formation of the diamine silver [Ag(NH₃)₂]⁺ complex in the presence of oxygen (eqn (3)).⁴¹ XPS of Ag 3d revealed an increase in full width half maxima (FWHM) of the peak after exposure to ammonia. This may have been due to oxidation of Ag or structural changes leading to peak broadening as atoms or molecules became more disordered (Fig. S11, ESI[†]).



This phenomenon was depicted by the presence of two peaks in a narrow scan of Ag of B and BT samples, which showed the presence of Ag⁰ as well as Ag⁺ that coordinated with the nitrogen atoms of the ammonia solution (Fig. 4A).^{42,43} The high-resolution XPS of N 1s also showed the presence of two peaks corresponding to neutral nitrogen (-N-H) from ammonia vapors at ~ 400 eV. The components at higher binding energy were most likely from positively charged nitrogen from NH₄OH (Fig. 4B).⁴⁴ Notably, the peak intensity of -N⁺ from NH₄OH increased after ammonia treatment in case of the hydrogel containing Au-bead@Ag nanorods (BT) as compared with that of the hydrogel with no Au-bead@Ag nanorods (CT). This phenomenon was due to the reaction of ammonia with H₂O

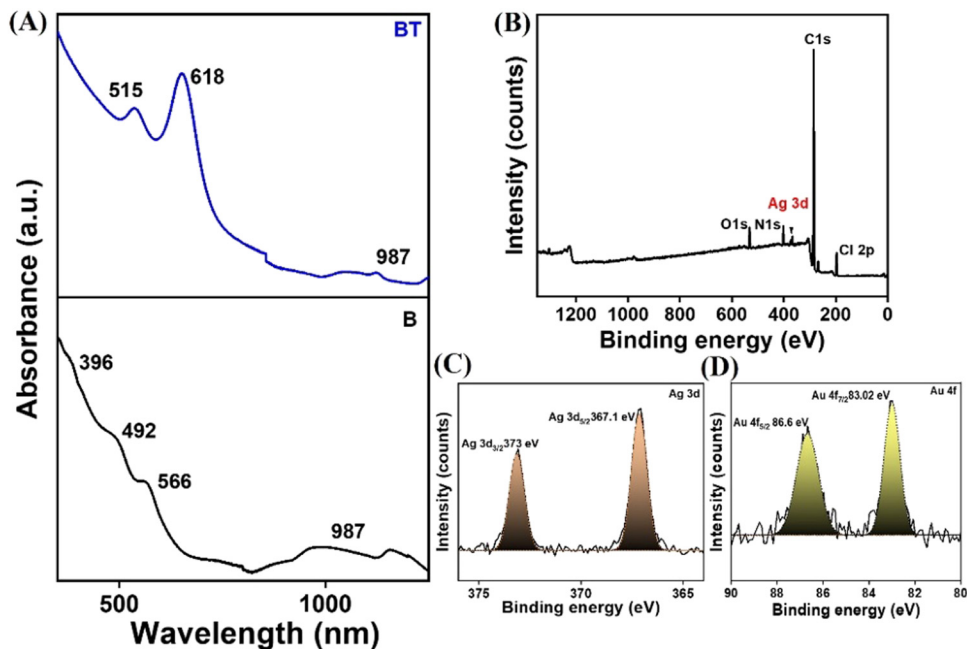


Fig. 3 (A) UV-Visible-NIR DRS of B (control-agarose hydrogel with Au-bead@Ag nanorods) and BT (control-agarose hydrogel with Au-bead@Ag nanorods) exposed to ammonia vapors, respectively. (B) XPS full survey scan of Au-bead@Ag nanorods. (C) and (D) High-resolution XPS spectrum of Ag 3d and Au 4f of Au-bead@Ag nanorods.

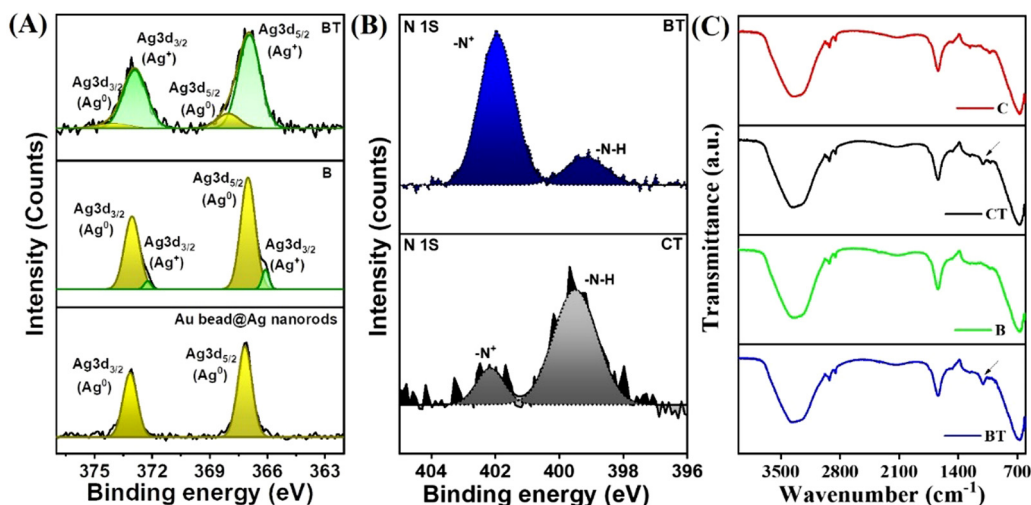


Fig. 4 (A) XPS narrow scan of Ag 3d. (B) Narrow scan of N 1s. (C) FTIR spectra of B (control-agarose hydrogel with Au-bead@Ag nanorods), BT (control-agarose hydrogel with Au-bead@Ag nanorods) exposed to ammonia vapors, C (control hydrogel (*i.e.*, agarose)), and CT (control agarose hydrogel) exposed to ammonia vapors.

present in the agarose gel (eqn (1)) as well as formation of the $[\text{Ag}(\text{NH}_3)_2]^+$ complex.

Thus, it can be concluded that the prepared edifice could entertain the interaction of volatile ammonia and Ag, which caused instability in the gel and aggregation of Au beads to ions, alloys, or clusters for a visual chromogenic change. Furthermore, FTIR spectroscopy also revealed the presence of a N–H wagging vibration in the hydrogel sensor after ammonia exposure (Fig. 4C).⁴⁵ It is worth noting that there was no color

change in the hydrogel containing Au beads only due to the stability of Au beads up to pH of 12 (Fig. S12, ESI[†]), as evident in previous reports.⁴⁶ However, in the case of Au-bead@Ag nanorods, formation of the $[\text{Ag}(\text{NH}_3)_2]^+$ complex along with the release of OH^- further increased the pH beyond 12, leading to the instability and aggregation of Au beads and Au–Ag hybrid. In conclusion, the transformation of Au-bead@Ag nanorods into clusters upon ammonia exposure was likely due to a combination of ammonia-induced silver dissolution

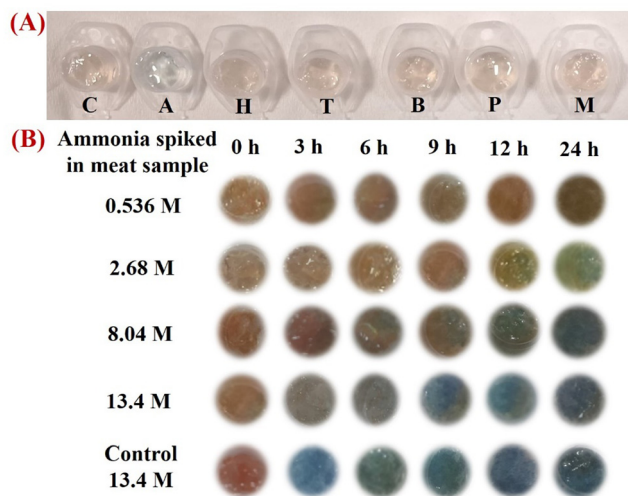


Fig. 5 (A) Interference study of the hydrogel sensor using different analytes. C = control agarose gel, A = ammonia, H = hydrazine, T = triethylamine, B = benzylamine, P = pyrrolidine, M = morpholine. (B) Colorimetric response for ammonia after spiking with different concentrations of ammonia in meat samples for different time intervals.

and structural destabilization, which led to aggregation and a red shift.

3.4 Selectivity and stability of the hydrogel sensor

We aimed to develop a sensor for the food-quality monitoring using ammonia detection, which arises at the final degradation of its derivatives (*e.g.*, amines). However, any perishable food is expected to release a number of amines through amino-acid degradation as well.⁴⁷ Hence, the color change of the hydrogel sensor should be specific to ammonia. Thus, it is pertinent to test it for the presence of other types of interfering molecule. These include biogenic amines such as trimethylamine, benzylamine, morpholine, hydrazine, and pyrrolidine, which can be released by the degradation of amino acids.³⁰ A significant color change was not observed in the presence of these interfering molecules at a concentration of 9 M (Fig. 5A). The reason behind the selectivity of the hydrogel for ammonia was the highest vapor pressure of ammonia and lowest boiling point as compared with those of all other molecules, as shown in Table 1. These features lead to its highly volatile nature, which caused its quick penetration within the gel. As the temperature increased, the kinetic energy of ammonia molecules rises, resulting in more rapid diffusion into the hydrogel and a quicker color change (Fig. S6, ESI[†]).⁴⁸ Additionally, it is a universal principle that the effective diffusion space varies with the size of the permeating molecule, and the effective diffusion length of a pore decreases as the size of the permeating molecule increases.⁴⁹ Moreover, the diffusion rate of analyte gases can be correlated to their molecular weight according to the Knudsen diffusion theory:

$$D = \frac{2r}{3} \sqrt{8RT} / \pi M$$

Table 1 Vapor pressure, boiling point and kinetic diameter of different types of interfering molecule

S. no.	Name of the molecule	Vapor pressure	Boiling point (°C)	Kinetic diameter ⁵¹ (nm)
1	Ammonia	1003 kPa	−33.34	0.421
2	Hydrazine	1 kPa	114	0.467
3	Triethylamine	6.899–8.506 kPa	89.28	0.761
4	Benzylamine	60 Pa	185	0.702
5	Pyrrolidine	6.51 kPa	87	0.639
6	Morpholine	0.79 kPa	129	3.649

where D is Knudsen diffusion constant, r is the pore radius, R is a gas constant, T is temperature, and M is gas mass.⁵⁰

Hence, ammonia having the least kinetic diameter as compared with other interfering molecules (Table 1) showed more selectivity to the developed hydrogel sensor.⁵¹ Another reason for the selectivity of the hydrogel sensor was difference in basicity.³⁰

The stability of hydrogel sensor after storing it at room temperature for a few days was also checked by exposing it to ammonia under identical conditions. The sensor showed almost the same color change without a significant change in its sensing performance compared with that of a newly formed sensor (Fig. S13, ESI[†]).

3.5 Application of the hydrogel sensor to ascertain the shelflife of meat

The selectivity of the sensor gel encouraged us to test the spoilage of fresh meat stored in a freezer for 2 days. The release of ammonia and exposure for 120 min is known to increase the pH and eventually spoil meat. It is hard to detect ammonia, particularly from stored frozen meat.⁵²

Therefore, the colorimetric response for ammonia after spiking ammonia in meat samples, which had been stored at 4 °C for 2 days, was evaluated. The sensor showed the same color change where the intensity increased gradually with time, as shown in Fig. 5B. This color change was linear with an increase in the concentration and time of spiking ammonia (0.536 M to 13.4 M) (Fig. S14, ESI[†]).

The applicability of the sensor was also checked by keeping it inside a tray containing 250 g of fresh chicken. There was a color change in the hydrogel sensor after 24 h (Fig. S15, ESI[†]). The time taken to change color was greater because ammonia will start to be released from the stored chicken after a certain period of time.

4. Conclusions

A chromogenic sensor using a non-toxic agarose hydrogel containing Au-bead@Ag nanorods was developed. The sensor could leach a thin layer of Ag and show a visual color change from orange to blue-green in the presence of volatile ammonia (~13.4 M) within 180 min at room temperature (25 °C) and 40% RH. Additionally, its performance demonstrated adaptability under varying environmental conditions, including temperature and humidity. The mechanism of the color change was confirmed with microscopic and spectroscopic methods.

Thus, the developed sensor could detect the ammonia released from the meat. This innovation offers a simple, highly sensitive, user-friendly, reliable, instrument-free, and cost-effective solution that is convenient and non-invasive for monitoring food safety and quality control in various scenarios.

Data availability

Data will be made available upon reasonable request.

Conflicts of interest

There are no conflicts to declare.

Acknowledgements

M. C. thanks INST for a fellowship and research facilities. V. S. thanks the Government of India DBT (BT/PR36476/NN/T/28/1723/2020). K. K. acknowledges DBT Biocare (BT/PR51368/BIC/101/1350/2023).

References

- WHO estimates of the global burden of foodborne diseases: foodborne diseases burden epidemiology reference group 2007–2015, <https://www.who.int/publications/item/9789241565165>, (accessed 6 January 2025).
- Y. Shigetomi, A. Ishigami, Y. Long and A. Chapman, *Nat. Commun.*, 2024, **15**, 1–11.
- C. O. Gill, *J. Food Prot.*, 1983, **46**, 444–452.
- P. Escobedo, M. M. Erenas, N. López-Ruiz, M. A. Carvajal, S. Gonzalez-Chocano, I. De Orbe-Payá, L. F. Capitán-Valley, A. J. Palma and A. Martínez-Olmos, *Anal. Chem.*, 2017, **89**, 1697–1703.
- J. Chen, J. Gu, R. Zhang, Y. Mao and S. Tian, *Sensors*, 2019, **19**, 605.
- P. F. M. Pereira, P. H. de Sousa Picciani, V. Calado and R. V. Tonon, *Trends Food Sci. Technol.*, 2021, **118**, 36–44.
- T. Lin, Y. Wu, Z. Li, Z. Song, L. Guo and F. Fu, *Anal. Chem.*, 2016, **88**, 11022–11027.
- S. Sutthasupa, C. Padungkit and S. Suriyong, *Food Chem.*, 2021, **362**, 130151.
- L. Wang, S. Xin, C. Zhang, X. Ran, H. Tang and D. Cao, *J. Mater. Chem. B*, 2021, **9**, 9383–9394.
- M. S. Steiner, R. J. Meier, A. Duerkop and O. S. Wolfbeis, *Anal. Chem.*, 2010, **82**, 8402–8405.
- A. Pacquitt, J. Frisby, D. Diamond, K. T. Lau, A. Farrell, B. Quilty and D. Diamond, *Food Chem.*, 2007, **102**, 466–470.
- P. Q. Leng, F. L. Zhao, B. C. Yin and B. C. Ye, *Chem. Commun.*, 2015, **51**, 8712–8714.
- R. Jagers and S. Bon, *J. Mater. Chem. B*, 2017, **5**, 8681–8685.
- J. Chen, A. A. Jackson, V. M. Rotello and S. R. Nugen, *Small*, 2016, **12**, 2469–2475.
- L. Song, Y. Zhu, Z. Yang, C. Wang and X. Lu, *J. Mater. Chem. B*, 2018, **6**, 5931–5939.
- G. Yang, Y. Lu, Y. Li, M. Ying, H. Pan, J. Qi and M. Du, *J. Mater. Chem. B*, 2021, **9**, 4663–4669.
- X. Li, S. Li, Q. Liu and Z. Chen, *Anal. Chem.*, 2019, **91**, 6315–6320.
- N. Fahimi-Kashani and M. R. Hormozi-Nezhad, *Anal. Chem.*, 2016, **88**, 8099–8106.
- X. Zhou, S. Huang, W. Liu and L. Shang, *Anal. Chem.*, 2024, **96**, 4224–4231.
- C. Pezzato, J. Chen, P. Galzerano, M. Salvi and L. Prins, *Org. Biomol. Chem.*, 2016, **14**, 6811–6820.
- X. Li and X. Su, *J. Mater. Chem. B*, 2018, **6**, 4714–4730.
- T. Shi, H. Lu, J. Zhu, X. Zhou, C. He, F. Li and G. Yang, *Composites, Part B*, 2023, **257**, 110687.
- Y. Wu, X. Yue, Y. Zhang, N. Yu, C. Ge, R. Liu, Z. Duan, L. Gao, X. Zang, X. Sun and D. Zhang, *Mater. Today Bio*, 2025, **30**, 101436.
- W. Qi, T. Li, Z. Zhang and T. Wu, *Food Hydrocolloids*, 2021, **110**, 106206.
- R. Jiang, F. Yang, X. Kang, X. Li, W. Jia, L. Pan and L. Yang, *Small*, 2025, **21**, 2570071.
- E. V. R. Campos, P. L. F. Proença, T. G. D. Costa, R. De Lima, S. Hedtrich, L. F. Fraceto and D. R. De Araujo, *ACS Appl. Polym. Mater.*, 2021, 4436–4449.
- X. Kang, L. Zhang, W. Jia, L. Yang and C. Jiang, *Anal. Chem.*, 2024, **96**, 20568–20577.
- J. Chu, Y. Zhang, J. Li, J. Hong, L. Sun and J. Wei, *J. Mater. Chem. B*, 2024, **12**, 7324–7333.
- P. Singh, T. A. F. König and A. Jaiswal, *ACS Appl. Mater. Interfaces*, 2018, **10**, 39380–39390.
- R. Jia, W. Tian, H. Bai, J. Zhang, S. Wang and J. Zhang, *Nat. Commun.*, 2019, **10**(10), 1–8.
- A. Orouji, F. Ghasemi, A. Bigdeli and M. R. Hormozi-Nezhad, *ACS Appl. Mater. Interfaces*, 2021, **13**, 20865–20874.
- K. Gopalakrishnan, M. Chandel, V. Gupta, K. Kaur, A. Patel, K. Kaur, A. Kishore, P. K. Prabhakar, A. Singh, J. S. Prasad, V. Bodana, V. Saxena, V. Shanmugam and A. Sharma, *Food Res. Int.*, 2023, **164**, 112321.
- K. Bhardwaj and A. Jaiswal, *Analyst*, 2023, **148**, 562–572.
- Y. Shin, I. T. Bae, B. W. Arey and G. J. Exarhos, *J. Phys. Chem. C*, 2008, **112**, 4844–4848.
- M. Shilpa, V. Shetty, S. Surabhi, J. R. Jeong, D. V. Morales, M. Ballal and S. C. Gurusurthy, *Mater. Sci. Eng., B*, 2023, **298**, 116893.
- I. Chummun Phul, M. A. L. Huët, D. Bekah and A. Bhaw-Luximon, *RSC Med. Chem.*, 2023, **14**, 534–548.
- E. Motamedi, B. Motesharezedeh, A. Shirinfekr and S. M. Samar, *J. Environ. Chem. Eng.*, 2020, **8**, 103583.
- A. K. Tamo, *J. Mater. Chem. B*, 2024, **12**, 7692–7759.
- C. J. Orendorff, T. M. Alam, D. Y. Sasaki, B. C. Bunker and J. A. Voigt, *ACS Nano*, 2009, **3**, 971–983.
- S. Malathi, T. Ezhilarasu, T. Abiraman and S. Balasubramanian, *Carbohydr. Polym.*, 2014, **111**, 734–743.
- Z. Qiu, Y. Xue, J. Li, Y. Zhang, X. Liang, C. Wen, H. Gong and J. Zeng, *Chin. Chem. Lett.*, 2021, **32**, 2807–2811.
- N. J. Firet, M. A. Blommaert, T. Burdyny, A. Venugopal, D. Bohra, A. Longo and W. A. Smith, *J. Mater. Chem. A*, 2019, **7**, 2597–2607.

- 43 C. Sun, C. Zhang, C. Jiang, C. Yang, Y. Du, Y. Zhao, B. Hu, Z. Zheng and K. O. Christe, *Nat. Commun.*, 2018, **91**, 1–7.
- 44 M. Šetka, R. Calavia, L. Vojkúvka, E. Llobet, J. Drbohlavová and S. Vallejos, *Sci. Rep.*, 2019, **91**, 1–10.
- 45 Vibrational Modes of Ammonia, <https://www.chem.purdue.edu/jmol/vibs/nh3.html>, (accessed 6 January 2025).
- 46 B. G. Ershov, E. V. Abkhalimov, R. D. Solovov and V. I. Roldughin, *Phys. Chem. Chem. Phys.*, 2016, **18**, 13459–13466.
- 47 J. M. Jay Modern food microbiology, 6th edn, Gaithersburg. https://scholar.google.com/scholar?hl=en&as_sdt=0%2C5&q=Jay+JM.+Modern+food+microbiology.+6th+ed.+Gaithersburg%3A+Aspen+Publishers%3B+2000.&btnG= (accessed 7 January 2025).
- 48 A. Chenite, S. Gori, M. Shive, E. Desrosiers and M. D. Buschmann, *Carbohydr. Polym.*, 2006, **64**, 419–424.
- 49 T. Yoshioka, M. Kanezashi and T. Tsuru, *AIChE J.*, 2013, **59**, 2179–2194.
- 50 M. Zhan, C. Ge, S. Hussain, A. S. Alkorbi, R. Alsaiari, N. A. Alhemiary, G. Qiao and G. Liu, *Chemosphere*, 2022, **291**, 132842.
- 51 Molecular Weight to Size Calculator – nanoComposix, <https://nanocomposix.com/pages/molecular-weight-to-size-calculator>, (accessed 20 March 2025).
- 52 Ammonia-Leaks On Meet PDF | PDF | Ammonia | Flavor, <https://www.scribd.com/document/440928748/Ammonia-leaks-on-meet-pdf>, (accessed 13 January 2025).